MCB
Journals.ASM.org

Binding of WIP to Actin Is Essential for T Cell Actin Cytoskeleton Integrity and Tissue Homing

Michel J. Massaad,[a] Michiko K. Oyoshi,[a] Jennifer Kane,[a] Suresh Koduru,[a]* Pilar Alcaide,[b]* Fumihiko Nakamura,[c] Narayanaswamy Ramesh,[a] Francis W. Luscinskas,[b] John Hartwig,[c] Raif S. Geha[a]

Division of Immunology, Children's Hospital, and Department of Pediatrics, Harvard Medical School, Boston, Massachusetts, USA[a]; Center for Excellence in Vascular Biology, Department of Pathology, Brigham and Women's Hospital, Harvard Medical School, Boston, Massachusetts, USA[b]; Division of Translational Medicine, Brigham and Women's Hospital, Harvard Medical School, Boston, Massachusetts, USA[c]

The Wiskott-Aldrich syndrome protein (WASp) is important for actin polymerization in T cells and for their migration. WASp-interacting protein (WIP) binds to and stabilizes WASp and also interacts with actin. Cytoskeletal and functional defects are more severe in WIP$^{-/-}$ T cells, which lack WASp, than in WASp$^{-/-}$ T cells, suggesting that WIP interaction with actin may be important for T cell cytoskeletal integrity and function. We constructed mice that lack the actin-binding domain of WIP (WIPΔABD mice). WIPΔABD associated normally with WASp but not F-actin. T cells from WIPΔABD mice had normal WASp levels but decreased cellular F-actin content, a disorganized actin cytoskeleton, impaired chemotaxis, and defective homing to lymph nodes. WIPΔABD mice exhibited a T cell intrinsic defect in contact hypersensitivity and impaired responses to cutaneous challenge with protein antigen. Adoptively transferred antigen-specific CD4$^+$ T cells from WIPΔABD mice had decreased homing to antigen-challenged skin of wild-type recipients. These findings show that WIP binding to actin, independently of its binding to WASp, is critical for the integrity of the actin cytoskeleton in T cells and for their migration into tissues. Disruption of WIP binding to actin could be of therapeutic value in T cell-driven inflammatory diseases.

The integrity of the actin cytoskeleton is important for T cell motility and migration into tissues (1), which is critical for immunosurveillance and defense against pathogens. The Wiskott-Aldrich syndrome protein (WASp) and its partner, the WASp-interacting protein (WIP), play important roles in the organization and function of the actin cytoskeleton in hematopoietic cells. These include the ability of T cells to polymerize F-actin, spread, chemotax, and form immune synapses following receptor ligation (2–8).

The WASp partner, WIP, is essential for WASp stability (9, 10). This is evidenced by the virtual absence of WASp in cells from WIP-deficient (*Wipf1*$^{-/-}$) mice and human despite normal levels of *Wasp* mRNA (9, 11). Furthermore, the WASp level is decreased in WAS patients with missense mutations in the WIP-binding domain of WASp (12) and is rescued by overexpression of a WIP peptide derived from the WASp-binding domain of WIP (13).

T cell cytoskeletal and functional defects are more severe in WIP-deficient than in WASp-deficient patients and mice. These include disruption of the actin filament network, impairment of proliferation to T cell receptor (TCR)/CD3 ligation, and defective chemotaxis (11, 14–16). These observations suggest that WIP is important for the integrity of the T cell actin cytoskeleton and T cell function, independently of stabilizing WASp.

WIP has an N-terminal verprolin homology (VH) region separated from the C-terminal WASp-binding domain by a central proline-rich region. The VH region of WIP shows high homology to the yeast actin-binding protein verprolin and has the motif KLKK (17) that is critical for actin binding to thymosin β4 (18). A purified glutathione *S*-transferase–WIP$_{1\text{-}127}$ fusion protein interacts with purified actin *in vitro* (17), demonstrating direct interaction between WIP and actin. This interaction is mediated by a 12-amino-acid sequence (amino acids 43 to 54) in WIP that includes the ^{45}KLKK^{48} motif (17). The addition of recombinant WIP to purified filamentous actin (F-actin) inhibits F-actin depolymerization *in vitro*, indicating that WIP stabilizes actin filaments (19). Deletion of WIP results in diminished F-actin in T cells from *Wipf1*$^{-/-}$ mice (14), while overexpression of WIP increases F-actin content in BJAB cells (10). Furthermore, transiently expressed WIP colocalizes with F-actin filaments in REF52.2 cells (20). These observations indicate that WIP interacts with and stabilizes F-actin and is important for the integrity of the actin cytoskeleton.

Since WASp is degraded in the absence of WIP, dissociating the WASp stabilizing function of WIP from its effects on the actin cytoskeleton has not been possible to date. To this purpose, we generated mice that lack the actin-binding domain (ABD) of WIP. Deletion of the ABD disrupted the association of WIP with F-actin but not with WASp and resulted in a defective actin cytoskeleton, diminished T cell chemotaxis, and impaired T cells homing to lymphoid organs and sites of antigen (Ag) challenge.

MATERIALS AND METHODS

Mice. The generation of WIPΔABD mice, which carry a homozygous deletion of 36 nucleotides in exon 2 of the endogenous *Wipf1* gene, is described in Fig. S1 in the supplemental material. WIPΔABD mice were

Received 21 April 2014 Returned for modification 30 May 2014
Accepted 12 September 2014
Published ahead of print 22 September 2014

Address correspondence to Raif S. Geha, raif.geha@childrens.harvard.edu.
* Present address: Suresh Koduru, School of Medical Sciences, University of Hyderabad, Hyderabad, India; Pilar Alcaide, Molecular Cardiology Research Institute, Tufts Medical Center, Tufts University School of Medicine, Boston, Massachusetts, USA.

Supplemental material for this article may be found at http://dx.doi.org/10.1128/MCB.00533-14.

doi:10.1128/MCB.00533-14

bred 10 generations on BALB/c and DO11.10 backgrounds and housed under pathogen-free conditions. Studies were performed in accordance with Boston Children's Hospital policies and procedures.

Immunoprecipitation assay. Splenocytes were lysed (1% Triton X-100, 100 mM Tris-Cl [pH 7.5], 50 mM NaCl), and lysates incubated with anti-WIP monoclonal antibody (MAb) 3D10 (21). Immune complexes were captured with protein G-Sepharose (GE Healthcare) and then denatured by boiling in sample buffer. Total lysates and immune complexes were separated on acrylamide gels and subjected to Western blot analysis. WIP was detected with anti-WIP MAb 3D10; WASp was detected with rabbit polyclonal antibody K374 (4); actin was detected with antiactin mouse MAb (Chemicon). The protein band intensities were quantified by using Adobe Photoshop.

F-actin sedimentation assay. Splenocytes were solubilized (1% Triton X-100, 100 mM KCl, 0.2 mM $MgCl_2$, 10 mM Tris-Cl [pH 7.5], 0.1 mM EGTA, 0.5 mM β-mercaptoethanol, 0.5 mM ATP, 1 μM phallacidin), precleared by slow-speed centrifugation of 10,000 × *g*, and then subjected to high-speed centrifugation of 400,000 × *g*. The pellet and supernatant of the high-speed centrifugation were denatured by boiling in sample buffer, separated on acrylamide gels, and subjected to Western blot analysis. WIP and actin were detected as described earlier; GAPDH (glyceraldehyde-3-phosphate dehydrogenase) was detected with anti-GAPDH MAb (Abcam). The protein band intensities were quantified by using Adobe Photoshop.

Flow cytometry. Single cell suspensions were surface stained or processed for intracellular staining using Fix&Perm cell permeabilization reagent (Invitrogen) and analyzed on LSRFortessa flow cytometer (BD Biosciences) and FlowJo software (Tree Star, Inc.). Antibodies included fluorescein isothiocyanate (FITC)-conjugated anti-CD3 (145-2C11), R-phycoerythrin (PE)-conjugated anti-CD4 (GK1.5), allophycocyanin (APC)-conjugated anti-CD8 (53-6.7), peridinin chlorophyll protein-cyanine dye (PerCP-Cy5.5)-conjugated anti-B220 (RA3-6B2), Alexa Fluor 647-conjugated anti-CCR7, PE-conjugated anti-CXCR4 (2B11), PE-conjugated anti-CD43 (1B11), PE-conjugated anti-LFA-1 (M17/4), PE-conjugated anti-CD11c (N418), FITC-conjugated anti-mouse TCR DO11.10 (KJ1-26), and Alexa Fluor 647-conjugated annexin V, all from eBioscience. The following antibodies were also used: rat anti-mouse PSGL-1 (2PH1; eBioscience), followed by PE-conjugated goat anti-rat IgG $F(ab')_2$ (Jackson Immunoresearch); biotin-conjugated rat anti-mouse VLA-4 (R1-2; BD Pharmingen), followed by PE-conjugated streptavidin (eBioscience); and rat anti-mouse CCR4 (kindly provided by Leonor Kremer, Centro Nacional de Biotecnología, Madrid, Spain), followed by DyLight488-conjugated goat anti-rat IgG $F(ab')_2$ (Jackson Immunoresearch). T cells purified by negative selection (Miltenyi) were either unstimulated or stimulated with anti-CD3 MAb (KT3; Serotec) and used for intracellular staining of F-actin filaments with FITC-conjugated phalloidin (Sigma).

Fluorescence and electron microscopy of the actin cytoskeleton. T cells were sedimented onto glass coverslips coated with 1 mg/ml poly-L-lysine (Sigma-Aldrich), poly-L-lysine, and 10 μg/ml anti-CD3 MAb (KT3; Serotec) or with poly-L-lysine and 1 μg/ml CCL19 (PrepoTech). Cells were stimulated for 30 min at 37°C, fixed with paraformaldehyde, and permeabilized with 0.5% Triton X-100 in phosphate-buffered saline (PBS), and F-actin was stained with TRITC (tetramethyl rhodamine isothiocyanate)-labeled phalloidin. Slides were viewed with a Nikon Eclipse E800 fluorescence microscope (Nikon) using a Plan Apo lens at 60× oil and 25°C. Images were acquired using a CoolSNAP EZ camera (Photometrics) and NIS-Elements BR 2.30 software (Nikon). Pictures were processed using Adobe Photoshop and Adobe Illustrator (Adobe). The cell surface area was measured using NIS-Elements BR 2.30 software.

For electron microscopy, T cells were sedimented onto glass coverslips coated with poly-L-lysine and 10 μg/ml anti-CD3 MAb. The adherent cells were stimulated 30 min at 37°C and then mechanically fractured by attaching a second poly-L-lysine-coated coverslip to the apical cell surface and removing it in PHEM buffer (60 mM PIPES, 25 mM HEPES, 10 mM EGTA, 2 mM $MgCl_2$, 1 μM phallacidin). Membrane fragments were washed with PHEM buffer, fixed in PHEM buffer containing 1% glutaraldehyde for 10 min, washed with distilled water, rapidly frozen, freeze-dried at −90°C, and coated with 1.5 nm of tantalum-tungsten at 25°C and 4 nm of carbon at 90°C. The replicas were removed with 12.5% hydrofluoric acid, washed with distilled water, picked up on carbon-Formvar-coated copper grids, and viewed in a JEOL-1200 EX electron microscope at 80 kV.

Live imaging microscopy. All live imaging experiments were performed at 37°C using a heated microscope chamber and prewarmed medium. Splenic T cells were sedimented on anti-CD3 coated surfaces and visualized with Nikon Eclipse T*i* microscope (Nikon). Images were captured every 10 s for 30 min using a CoolSNAP HQ^2 camera (Photometrics) and NIS-Elements AR3.2 software (Nikon).

***In vitro* chemotaxis assay.** *In vitro* chemotaxis was assayed using transwell chambers (6.5-mm diameter, 5-μm pore size; Costar). A total of 10^6 purified splenic T cells in 100 μl of RPMI 1640 with 1% fetal calf serum (FCS) was added to the upper chamber, and 600 μl of RPMI 1640 with 1% FCS with or without 50, 100, or 500 ng/ml CCL19 or 50 ng/ml SDF-1α (PrepoTech) was added to the bottom chamber. After 3 h at 37°C, cells that migrated to the lower chamber were collected and counted. The experiments were performed in duplicate on three mice in each group.

***In vivo* homing of T cells.** T cells were purified from spleens. Wild-type (WT) T cells were labeled 15 min at 37°C with 20 μg/ml carboxylic acid succinimidyl ester-Alexa Fluor 488 (green dye) or carboxylic acid succinimidyl ester-Alexa Fluor 555 (red dye). WIPΔABD T cells were labeled with carboxylic acid succinimidyl ester-Alexa Fluor 555. Labeled cells were then washed and suspended in RPMI 1640. Ten million Alexa Fluor 488-labeled WT T cells were mixed either with 10^7 Alexa Fluor 555-labeled WT T cells or 10^7 Alexa Fluor 555-labeled WIPΔABD T cells. Cells were intravenously (i.v.) injected into WT recipient mice and, 1 h later, the mice were sacrificed, and blood and lymph nodes (LNs) were harvested. Single-cell suspensions were analyzed by flow cytometry, and the percentage of Alexa Fluor 488^+ and Alexa Fluor 555^+ cells were determined. The T cell homing index was calculated as the ratio of Alexa Fluor 555^+ to Alexa Fluor 488^+ cells and divided by the ratio of WT to WT cells.

T cell proliferation and cytokine production. Purified T cells were stimulated 72 h with immobilized anti-CD3 MAb. A total of 1 μCi of tritiated thymidine was added, and the cultures were incubated for an additional 16 h. Proliferation was determined by the incorporation of tritiated thymidine into cellular genomic DNA. Radioactivity was detected on a Trilux 1450 MicroBeta counter after transfer to Filtermat A and the addition of liquid scintillation cocktail (Perkin-Elmer). Total splenocytes from WT or WIPΔABD mice on the DO11.10 background were stimulated with $OVA_{323-339}$ peptide (Bachem), and their proliferation was determined as described above. Mice were anesthetized with 2,2,2-tribromoethanol (Sigma), immunized intraperitoneally (i.p.) on day 0 with 10 μg/mouse keyhole limpet hemocyanin (KLH; Biosearch Technologies, Inc.) in alum (Thermo Scientific), and then boosted on days 7 and 14 with 2.5 μg/mouse KLH. On day 21, the mice were sacrificed, the splenocytes were stimulated with KLH, and their proliferation determined as described above. Levels of interleukin-2 (IL-2), IL-13, and gamma interferon (IFN-γ) in the culture supernatants were measured by enzyme-linked immunosorbent assay (eBioscience).

RNA preparation, cDNA synthesis, and quantitative real-time PCR. Ears were homogenized in TRIzol (Gibco) using a Polytron RT-3000 (Kinematica). RNA was extracted and used for cDNA synthesis using iScript cDNA synthesis kit (Bio-Rad). mRNA for *Il4*, *Il13*, and *Ifn*γ was quantified on ABI7700 real-time PCR system using TaqMan primers/probe (Applied Biosystems) and normalized with the mouse β_2-*microglobulin* gene.

***In vivo* DC migration and *in vitro* DC function.** Mice were anesthetized and painted on shaved back skin with 1 mg of FITC in 100 μl of 1:1 acetone-dibutylpthalate (Sigma). Draining LNs (DLNs) were collected 24 h later, and $FITC^+$ dendritic cells (DCs) were measured by flow cytometry. For DC function, mice were subjected to epicutaneous (EC) sensiti-

zation as follows. Mice were anesthetized, and then their dorsal skin was shaved and taped-stripped with transparent bio-occlusive dressing (Tegaderm). Ovalbumin (OVA; 200 μg; Sigma) or PBS was placed on sterile gauze that was secured to the skin with a dressing. DCs were purified 24 h later from DLNs (Miltenyi) and used to present OVA to naive T cells purified from WT DO11.10 mice, without the further addition of OVA Ag. Proliferation of and cytokine production by DO11.10 T cells was assessed as described above.

Measurement of *in vitro* T cell adhesion under defined flow conditions. T cell interaction with immobilized adhesion molecules was observed by videomicroscopy (20× objective) under defined laminar flow conditions in a parallel-plate apparatus (22). Glass coverslips were coated with 20 μg/ml recombinant VCAM-1 or ICAM-1 (R&D Systems). SDF-1α (2 μg/ml) was added to the ICAM-1-coated coverslips 15 min before perfusion of the T cells to facilitate T cell LFA-1 integrin activation and binding to ICAM-1. Accumulation of T cells on immobilized molecules was determined using Videolab software (Ed-Marcus Laboratories) by counting adherent T cells in eight different fields after the initial minute of shear flow at 1 dyn/cm^2.

Contact hypersensitivity to hapten and histological analysis. Anesthetized mice were sensitized on shaved abdominal skin with 100 μl of 2% oxazolone (Sigma) in ethanol on day 1 or 25 μl of 0.5% DNFB (Sigma) in acetone-olive oil (4:1) on days 0 and 1. On day 5, one ear was challenged with 10 μl of 1% oxazolone or 20 μl of 0.25% DNFB, and the second ear was challenged with vehicle. Ear thickness was measured after 24, 48, 72, and 96 h with a micrometer (Mitutoyo). Alternatively, T cells were purified from the spleens of mice that were sensitized 6 days with DNFB, and 10^7 cells were injected into naive mice that were immediately challenged on their ears with DNFB or vehicle alone. For histological analysis, ear skin was obtained 24 h after challenge, fixed in 10% buffered formalin, and embedded in paraffin. Multiple 4-μm sections were stained with hematoxylin and eosin (H&E) and then visualized by light microscopy.

EC sensitization of mice and secondary site challenge. Mice were subjected to two rounds of EC sensitization with 100 μg of OVA on the first week, followed by a 2-week rest period. This cycle was repeated three times and, at the end of the third cycle, mice were challenged by intradermal (i.d.) injection in the ear of 20 μl of 1:1 mixture of 25 μg of $OVA_{323-339}$ peptide in PBS with 100 ng of pertussis toxin (PT; List Biological Laborarories, Inc.) and incomplete Freund adjuvant (IFA; Sigma). PBS-PT-IFA was injected in the second ear of the same mouse as control. Seven days later, single-cell suspensions were prepared from the ears and stained for CD3/CD4 after excluding dead cells using the viability dye eFluor 506.

Adoptive transfer of activated DO11.10 CD4$^+$ cells and skin challenge. Splenocytes were stimulated 5 days with 300 μg/ml OVA protein and 20 ng/ml recombinant mouse IL-2 (R&D Systems). Purified CD4$^+$ cells were stained with CellTrace (Molecular Probes) and 15 × 10^6 cells were adoptively transferred to naive WT or WIPΔABD BALB/c recipients, which were challenged the same day by i.d. injection in one ear of 20 μl of a 1:1 mixture of 25 μg of $OVA_{323-339}$ peptide in PBS plus 100 ng of PT-IFA. PBS-PT-IFA was injected in the second ear of the same mouse as a control. Seven days later, single-cell suspensions were prepared from the ears and stained for CD4, KJ1-26, and annexin V.

Statistical analysis. Statistical analysis of the data using Student *t* test or two-way analysis of variance for multiple groups was performed with Prism software.

RESULTS

Generation of knock-in mice with deletion of the ABD of WIP. The strategy to generate mice with homozygous deletion of the ABD of WIP is depicted in Fig. S1 in the supplemental material. WIPΔABD mice carry a homozygous deletion of 36 nucleotides in exon 2 of the endogenous *Wipf1* gene, which encode amino acids 43 to 54 in WIP (Fig. 1A). Similar findings were obtained in all experiments with WIPΔABD mice generated from two independently targeted ES clones.

WIPΔABD mice did not differ in growth, weight, or health from their wild-type (WT) littermates. WIPΔABD mice had normal thymus and bone marrow cellularity. Furthermore, they had normal T and B cell development except for an increase in CD43^{low} B220^{low} pre-B cells and IgM$^+$ B220^{low} immature B cells (see Fig. S2 in the supplemental material).

WIPΔABD protein exhibits normal interaction with WASp but decreased association with F-actin. Examination of splenocyte lysates revealed that WIPΔABD migrated at a slightly lower molecular weight than WT WIP (Fig. 1B) and that its level was not significantly decreased compared to intact WIP (Fig. 1C), indicating that deletion of the ABD domain does not significantly affect the stability of WIP. Splenocytes from WIPΔABD mice did not exhibit a significant decrease in the level of WASp compared to WT mice (Fig. 1B and C). The WIP/WASp ratio was comparable in WIPΔABD mice and WT controls. Moreover, WASp coimmunoprecipitated with WIPΔABD to a comparable extent as it did with WT WIP (Fig. 1D), indicating that deletion of the ABD does not affect the ability of WIP to interact with and stabilize WASP.

To examine the impact of deleting the ABD on the ability of WIPΔABD to associate with F-actin in cells, splenocytes from WIPΔABD mice and WT controls were solubilized in a buffer containing phalloidin to stabilize F-actin, after which lysates were subjected to high-speed centrifugation. About 30% of WIP cosedimented with F-actin in the pellet from WT cells (Fig. 1E and F). In contrast, only ~12% of WIPΔABD cosedimented with F-actin in the pellet from WIPΔABD cells. The fraction of actin that sedimented in the high-speed pellet was decreased by ~14% in WIPΔABD cells compared to WT controls (Fig. 1F). The WIP/F-actin ratio in the pellet was significantly lower in splenocytes from WIPΔABD mice than WT controls. These results indicate that deletion of the ABD impairs the ability of WIP to associate with F-actin in cells.

The ABD of WIP is important for maintaining cellular F-actin content and for actin cytoskeleton integrity in T cells. T cells from WIPΔABD mice had a significantly decreased level of intracellular F-actin compared to WT T cells (Fig. 2A). However, the relative increase in F-actin content following TCR/CD3 cross-linking was comparable in WIPΔABD and WT T cells (Fig. 2B). These results indicate that the ABD of WIP is important for maintaining the baseline level of cellular F-actin but not for TCR/CD3-driven F-actin polymerization.

TCR/CD3 ligation results in reorganization of the actin cytoskeleton in T cells (4, 23). To examine TCR/CD3-driven actin cytoskeleton reorganization, purified T cells were allowed to spread on coverslips coated with anti-CD3 MAb and permeabilized, and then their F-actin was stained with TRITC-phalloidin and visualized by fluorescence microscopy. Unstimulated T cells had a round shape with a peripheral ring of F-actin (Fig. 2C). WT T cells stimulated with anti-CD3 polarized F-actin and extended microspikes and blunt pseudopodia enriched in F-actin (Fig. 2C and D). In contrast, T cells from WIPΔABD mice spread poorly over anti-CD3-coated coverslips, and failed to extend microspikes or pseudopodia, resulting in significantly lower cell surface area compared to WT T cells (Fig. 2E). These results indicate that the ABD of WIP is important for actin cytoskeletal reorganization in T cells following TCR/CD3 ligation.

Time-lapse microscopy was used to visualize the motility of live T cells placed on anti-CD3-coated surface, an experimental system that mimics T cell activation by antigen-presenting cells

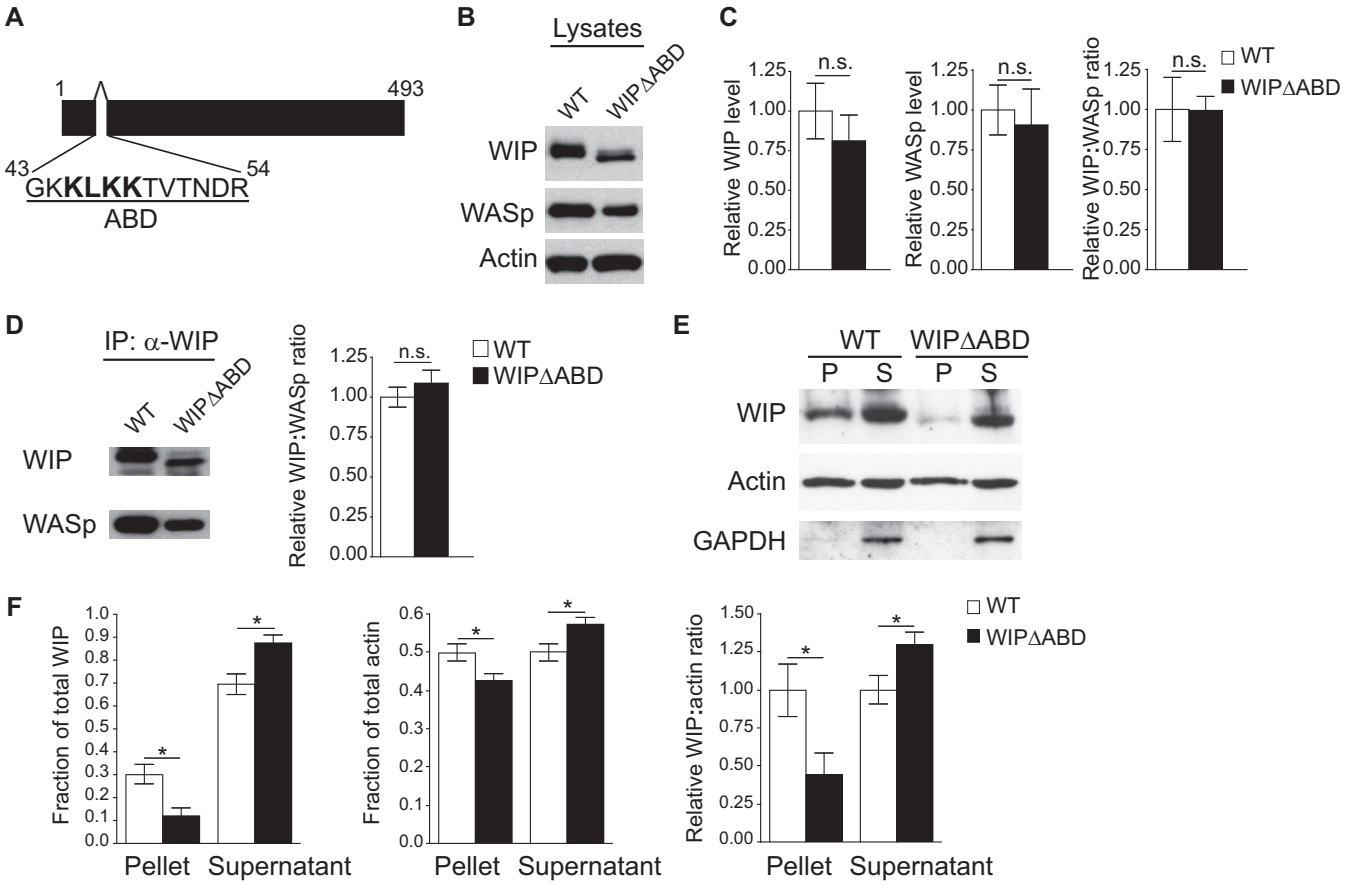

FIG 1 The WIPΔABD mutant exhibits impaired cosedimentation with F-actin but a normal association with WASp. (A) Schematic representation of the WIP sequence with the deleted actin-binding domain (ABD) shown. (B) Representative Western blot of WIP, WASp, and actin in splenocyte lysates from WIPΔABD mice and WT controls. Similar results were obtained in five independent experiments. (C) Quantification of WIP and WASp levels relative to actin and of the WIP/WASp ratio in splenocytes from WIPΔABD mice and WT controls, normalized to a value of 1.0 for the WT controls ($n = 5$ for each group). (D) Representative Western blot analysis of WIP and WASp (left panel), and quantitative analysis of the WIP/WASp ratio (right panel) in WIP immunoprecipitates from splenocyte lysates of WIPΔABD mice and WT controls. The WIP/WASp ratio in WT controls was set at 1.0 ($n = 3$ for each group). (E) Representative Western blot analysis of WIP and actin in the high-speed centrifugation pellet (P) and supernatant (S) of splenocyte lysates from WIPΔABD mice and WT controls. GAPDH was used to rule out contamination of the P fraction with soluble proteins. Similar results were obtained in five independent experiments. (F) Quantitation of the fractions of WIP and actin, and of the WIP/actin ratio in the high-speed centrifugation pellet and supernatant of splenocyte lysates from WIPΔABD mice and WT controls. The WIP/WASp ratio in WT controls was set at 1.0 ($n = 5$ for each group). Columns and bars represent means ± the standard errors of the mean (SEM). *, $P < 0.05$; n.s., not significant.

(APCs) (24). WT T cells extended and retracted dynamic pseudopodia over the time course of the observation period (see Movie S1 in the supplemental material). In contrast, WIPΔABD T cells were less motile and displayed smaller pseudopodia than WT T cells (see Movie S2 in the supplemental material). Thus, the ABD of WIP is essential for normal actin cytoskeleton-dependent T cell dynamics following TCR ligation.

To evaluate the ultrastructure of the actin cytoskeleton, purified T cells were spread on anti-CD3-coated coverslips; their apical surface was then removed, and the attached cell membranes were processed for electron microscopy (EM). EM images of the cytoplasmic side of the adherent plasma membranes revealed that the amount of F-actin associated with the inner side of the plasma membrane in WIPΔABD T cells was greatly diminished compared to WT T cells (Fig. 2F). In addition, the F-actin filaments were significantly shorter and less dense (Fig. 2G). These results indicate that the ABD of WIP is important for the integrity of the cortical actin cytoskeleton in T cells.

The ABD of WIP is important for T cell chemotaxis and homing to lymphoid organs. Cytoskeletal integrity is critical for the migration of T cells in response to a chemokine gradient. After stimulation with CCL19, WIPΔABD T cells upregulated F-actin normally (Fig. 3A); however, the percentage of WIPΔABD T cells that exhibited a polarized migratory morphology (defined as actin-rich structures at the leading edge and/or within a constricted uropod) was markedly decreased compared to WT T cells (Fig. 3B and C). T cells from WIPΔABD mice had a significantly reduced chemotactic response to CCL19 and SDF-1α compared to WT T cells (Fig. 3D and data not shown), despite normal surface expression of CCR7 and CXCR4, the receptors for CCL19 and SDF-1α (Fig. 3E and data not shown). These results suggest that the ABD of WIP is essential for T cell chemotaxis.

CCL19 and SDF-1α play important roles in the migration of T cells from the circulation into LNs (25–28). We compared the ability of T cells from WIPΔABD mice and WT controls to home to the LNs of WT recipients. Equivalent numbers of Alexa Fluor

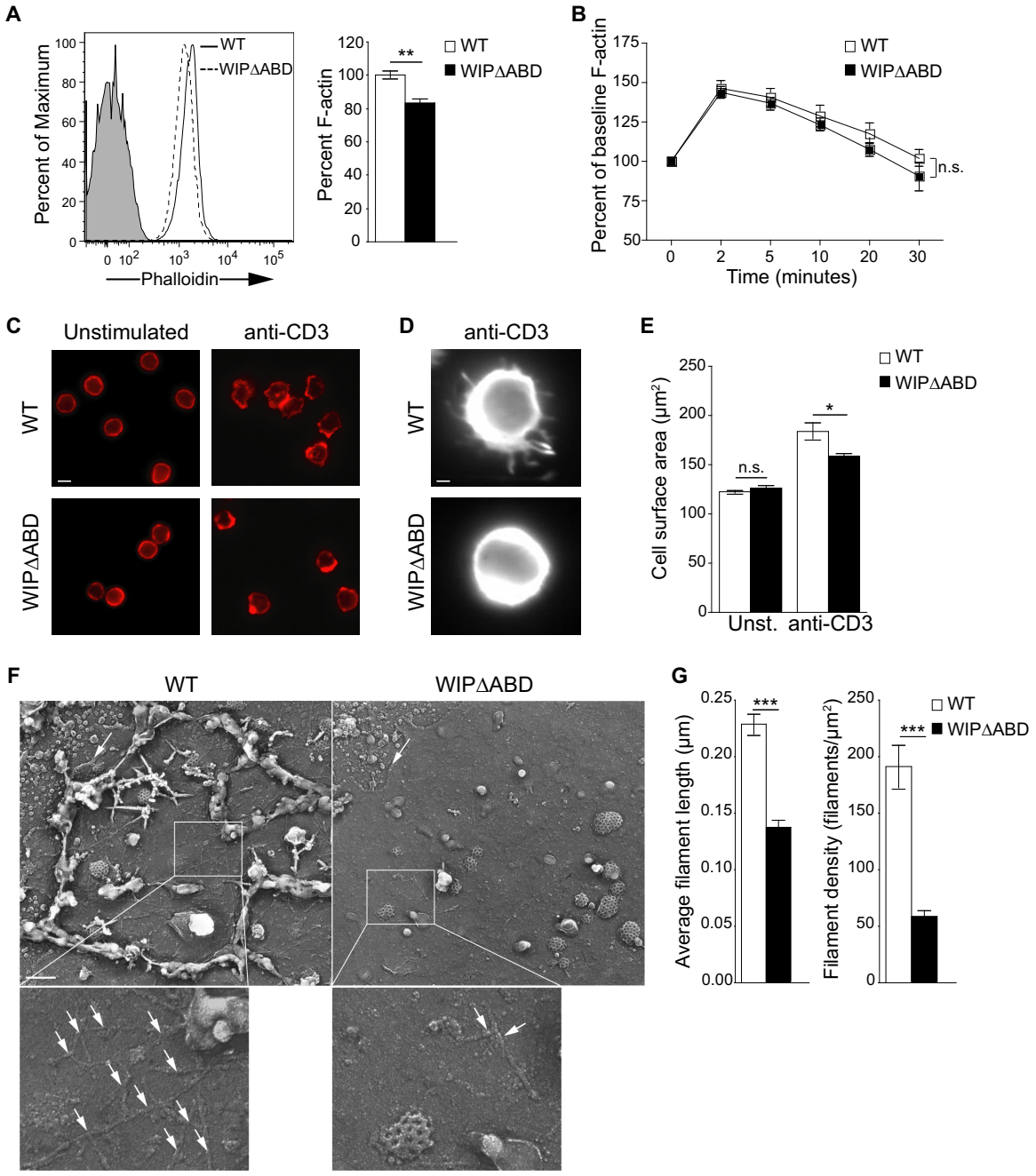

FIG 2 Decreased F-actin content and defective actin cytoskeleton rearrangement and integrity in WIPΔABD T cells. (A) Representative fluorescence-activated cell sorting (FACS) analysis of TRITC-phalloidin staining for F-actin in resting T cells and quantitative analysis of the results as a percentage of the WT controls ($n = 3$). The solid gray curve in the histogram represents the isotype control. (B) F-actin increase in T cells following stimulation with anti-CD3 MAb. The results are expressed as a percentage of the baseline for each group ($n = 3$). (C) Intracellular fluorescence of TRITC-phalloidin in T cells stimulated with anti-CD3 MAb ($n = 3$). Bar, 10 μm. (D) Magnification of one T cell stimulated with anti-CD3 MAb. Bar, 1 μm. (E) Cell surface area of T cells following stimulation with anti-CD3 MAb ($n = 3$). Unst., unstimulated. A total of 90 cells per condition were counted in each experiment. (F) Representative metal cast electron microscope images of the apical membrane of T cells stimulated with anti-CD3 MAb. Shown are the cytoskeletal actin fibers associated with the cytoplasmic side of the adherent plasma membranes. Clathrin-coated pits can also be seen. The arrows indicate the edge of the cell membrane. Bar, 200 nm. The magnified areas show the actin filaments (arrows) associated with the plasma membranes. (G) Actin filament length and density in T cell membranes from WIPΔABD mice and WT controls visualized in panel F ($n = 2$ for each group). F-actin was measured in 190 WT T cells and 80 WIPΔABD T cells. Columns or squares and bars represent means ± the SEM. ***, $P < 0.0001$; **, $P < 0.01$; *, $P < 0.05$; n.s., not significant.

555-labeled WIPΔABD T cells or control WT T cells were mixed with Alexa Fluor 488-labeled WT T cells and i.v. injected into recipients. An hour later, the percentage of transferred WT and WIPΔABD T cells were analyzed in the blood and LNs of WT recipients by flow cytometry (Fig. 3F and G). The homing index was calculated as the ratio of Alexa Fluor 555-labeled to Alexa Fluor 488-labeled cells and normalized to the ratio of WT controls. The homing of WIPΔABD T cells to cervical, axillary, ingui-

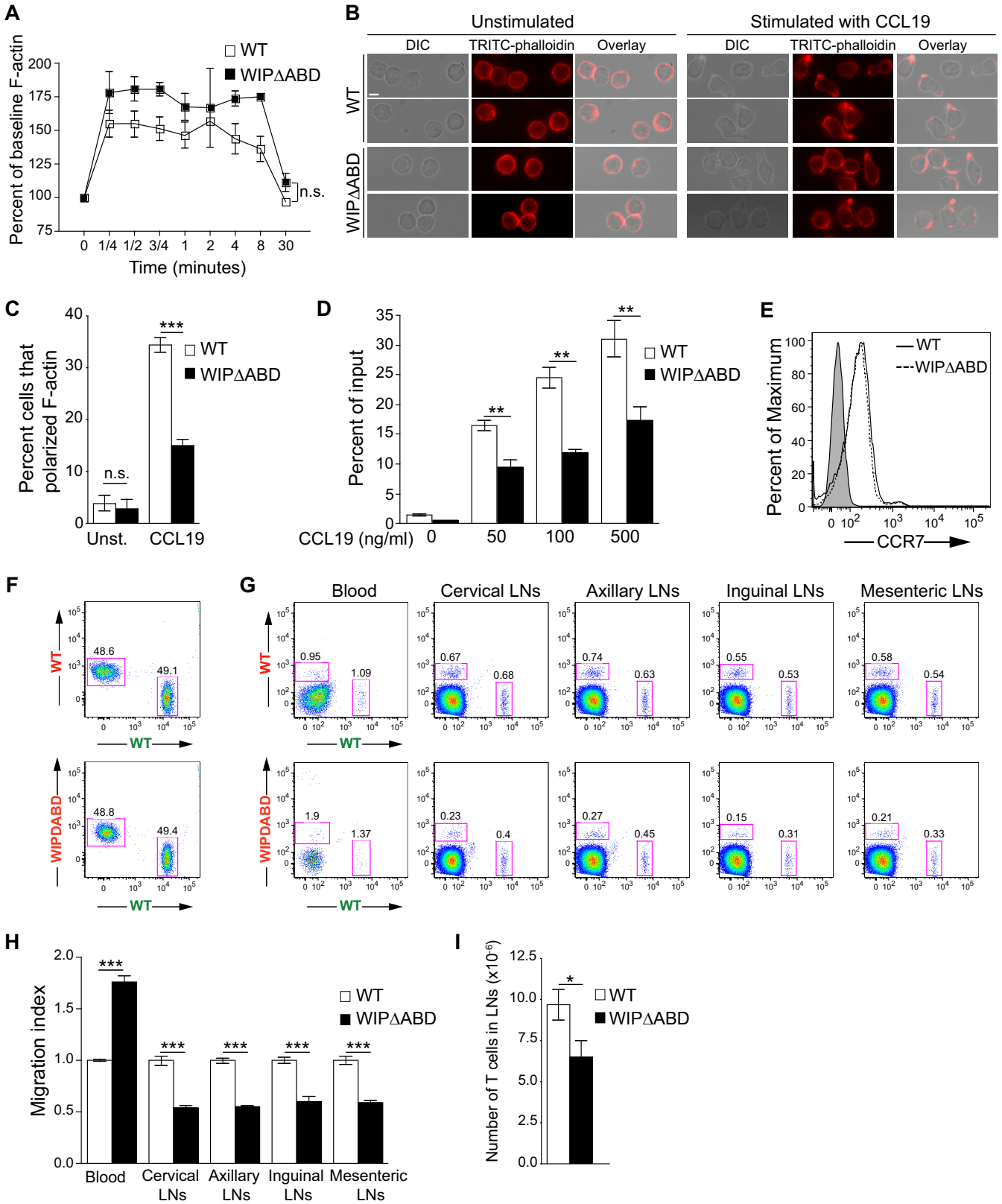

FIG 3 Defective *in vitro* migration and *in vivo* homing of WIPΔABD T cells. (A) F-actin increase in WIPΔABD and WT T cells following stimulation with CCL19. The results are expressed as the percentage of the baseline for each group ($n = 3$). (B) Differential interference contrast (DIC) images of the cells, TRITC-phalloidin images of F-actin, and an overlay of DIC and TRITC-phalloidin fluorescence images of WIPΔABD and WT T cells show the cellular location of the actin-rich structures at the leading edge and/or in the uropods. Two representative images for each condition are shown. Stimulation with CCL19 resulted in F-actin polarization in three of four (upper panel) and two of two (lower panel) WT T cells shown. In contrast, one of five (upper panel) and one of three (lower

nal, and mesenteric LNs was significantly decreased compared to WT T cells (Fig. 3H). Conversely, WIPΔABD T cells were retained in the circulation significantly more than WT T cells. Similar results were obtained when WT T cells were labeled with Alexa Fluor 555, and WT or WIPΔABD T cells were labeled with Alexa Fluor 488 prior to i.v. injection into WT recipients (see Fig. S3 in the supplemental material). Consistent with the impaired homing of the T cells from the mutant, the number of T cells in inguinal and axillary LNs was significantly lower in WIPΔABD mice compared to WT controls (Fig. 3I). These results indicate that the ABD of WIP in important for optimal homing of T cells to secondary lymphoid organs.

Normal intrinsic T cell function but impaired contact hypersensitivity (CHS) in WIPΔABD mice. Proliferation and secretion of IFN-γ were comparable in splenic T cells from WIPΔABD mice and WT controls (Fig. 4A). Furthermore, after i.p. immunization with keyhole limpet hemocyanin (KLH), splenocyte proliferation and secretion of IFN-γ in response to stimulation with KLH Ag were comparable in WIPΔABD mice and WT controls (Fig. 4B). These results indicate that intrinsic T cell function and T cell priming in response to i.p. immunization are intact in WIPΔABD mice.

T cells are important for the development of CHS reactions to hapten (29, 30). We examined the ability of WIPΔABD mice to mount a CHS reaction to the hapten dinitrofluorobenzene (DNFB). Six days after hapten sensitization, mice were challenged with hapten on one ear and with vehicle on the other ear. WIPΔABD mice developed significantly less ear thickening in response to DNFB challenge than WT controls (Fig. 4C). Histologic examination of the ears revealed less edema and cellular infiltration in WIPΔABD mice (Fig. 4D). Moreover, there were significantly smaller amounts of mRNA for *Ifn*γ and *Il4* in the hapten-challenged ears of WIPΔABD mice compared to WT controls (Fig. 4E). Similar results were obtained using the hapten oxazolone (see Fig. S4 in the supplemental material). These findings demonstrate that the ABD of WIP is important for CHS.

To determine whether the impaired CHS response in WIPΔABD mice is T cell intrinsic, WIPΔABD mice and WT controls were sensitized with DNFB. Six days later, splenic T cells were adoptively transferred into WT or WIPΔABD recipients that were challenged on one ear with DNFB and on the other with vehicle alone. Adoptive transfer of T cells from WT donors elicited a comparable CHS response in WT and WIPΔABD recipients (Fig. 4F). In contrast, adoptive transfer of T cells from WIPΔABD donors failed to elicit a CHS response in both WT and WIPΔABD recipients. These results suggest that T cells are the major contributors to the impaired CHS response in WIPΔABD mice.

WIPΔABD mice mount a normal T effector response to cutaneous sensitization with ovalbumin but fail to respond to secondary cutaneous antigen challenge. The failure of WIPΔABD mice to mount a CHS response could be due to failure to generate a T cell response to the hapten and/or to failure of T effector cells to migrate to the site of hapten challenge. Because T cell responses to haptens are difficult to measure, we examined the response of the mutant to epicutaneous (EC) sensitization and challenge with ovalbumin (OVA). Mice were EC sensitized by the application of OVA patches to tape-stripped skin as previously described (31). Proliferation and secretion of IL-2, IFN-γ, and IL-13 by splenocytes in response to stimulation with OVA Ag were comparable in WIPΔABD mice and WT control mice (Fig. 5A). The systemic response to EC sensitization is dependent on the migration of Ag-laden skin DCs to the DLN (32, 33). The numbers of $CD11c^+$ $FITC^+$ DCs in the DLNs of FITC-painted tape-stripped skin were normal in WIPΔABD mice (see Fig. S5A in the supplemental material), as previously reported in *Wipf1*$^{-/-}$ mice (16). Furthermore, WIPΔABD DCs from tape-stripped mice were able to present OVA and induce T cell proliferation and IL-2, IFN-γ, and IL-13 production by naive WT T cells purified from DO11.10 mice (see Fig. S5B in the supplemental material). These results indicate that the ABD of WIP is not essential for the induction of an effector T cell response to cutaneous sensitization.

To investigate the ability of T effector cells to respond to a cutaneous challenge, mice EC sensitized on the back with OVA were challenged i.d. with OVA in one ear and PBS in the other ear. Ears were analyzed 7 days later for the presence of $CD3^+$ $CD4^+$ cells and for cytokine mRNA expression. Ear challenge of WT mice with OVA caused accumulation of $CD3^+$ $CD4^+$ cells (Fig. 5B and C) and increased expression of *Ifn*γ and *Il13* mRNA compared to challenge with PBS (Fig. 5D). In contrast, there was no significant increase in $CD3^+$ $CD4^+$ cells or expression of mRNA for *Ifn*γ and *Il13* in the OVA-challenged ears of WIPΔABD mice. These results indicate that WIPΔABD mice are impaired in their ability to mount an inflammatory response to Ag challenge at a secondary skin site.

Impaired homing of WIPΔABD T cells to sites of cutaneous Ag challenge. We used an adoptive transfer model to directly examine the capacity of T effector cells from WIPΔABD mice to home to OVA-challenged skin. Splenocytes from WIPΔABD and WT mice on the DO11.10 background were stimulated with OVA for 5 days, and then $CD4^+$ cells were purified and used for adoptive transfer. The proliferation and secretion of IL-2 and IFN-γ were comparable in the two strains (Fig. 6A). Furthermore, Ag-activated $CD4^+$ cells expressed comparable amounts of the skin homing receptor CCR4, the selectin ligands CD43 and PSGL-1, and the integrins LFA-1 and VLA-4 (Fig. 6B and C). In addition,

panel) WIPΔABD T cells show clear F-actin polarization upon stimulation with CCL19 ($n = 3$). Bar, 10 μm. (C) Percentages of WIPΔABD and WT T cells that polarize F-actin following stimulation with CCL19 ($n = 3$). Unst., unstimulated. A total of 180 cells per condition were counted in each experiment. (D) Migration of splenic T cells from WIPΔABD mice and WT controls toward CCL19. The percentage of cells in the lower compartment of a transwell chamber is shown ($n = 3$ for each group). (E) Representative FACS analysis of CCR7 expression on the surface of splenic T cells purified from WIPΔABD mice and WT controls. Shaded histogram represents the isotype control ($n = 3$ for each group). (F) Representative FACS analysis of a mixture of equal numbers of Alexa Fluor 488-labeled WT T cells (designated by green lettering) and Alexa Fluor 555-labeled WT or WIPΔABD T cells (designated by red lettering) used for injection into genetically matched WT recipients. (G) Representative FACS analysis of cells from the blood and LNs of WT recipients obtained 1 h after i.v. administration of a 1:1 mixture of equal numbers of Alexa Fluor 488-labeled WT T cells (designated by green lettering) and Alexa Fluor 555-labeled WT or WIPΔABD T cells (designated by red lettering). (H) Quantitative analysis of the homing index of WIPΔABD T cells relative to the mean homing index of WT T cells set at 1.0 ($n = 5$ for each group). (I) T cell numbers in the inguinal and axillary LNs of WIPΔABD mice and WT controls ($n = 6$ for each group). Columns and bars represent means ± SEM. ***, $P < 0.0001$; **, $P < 0.01$; *, $P < 0.05$.

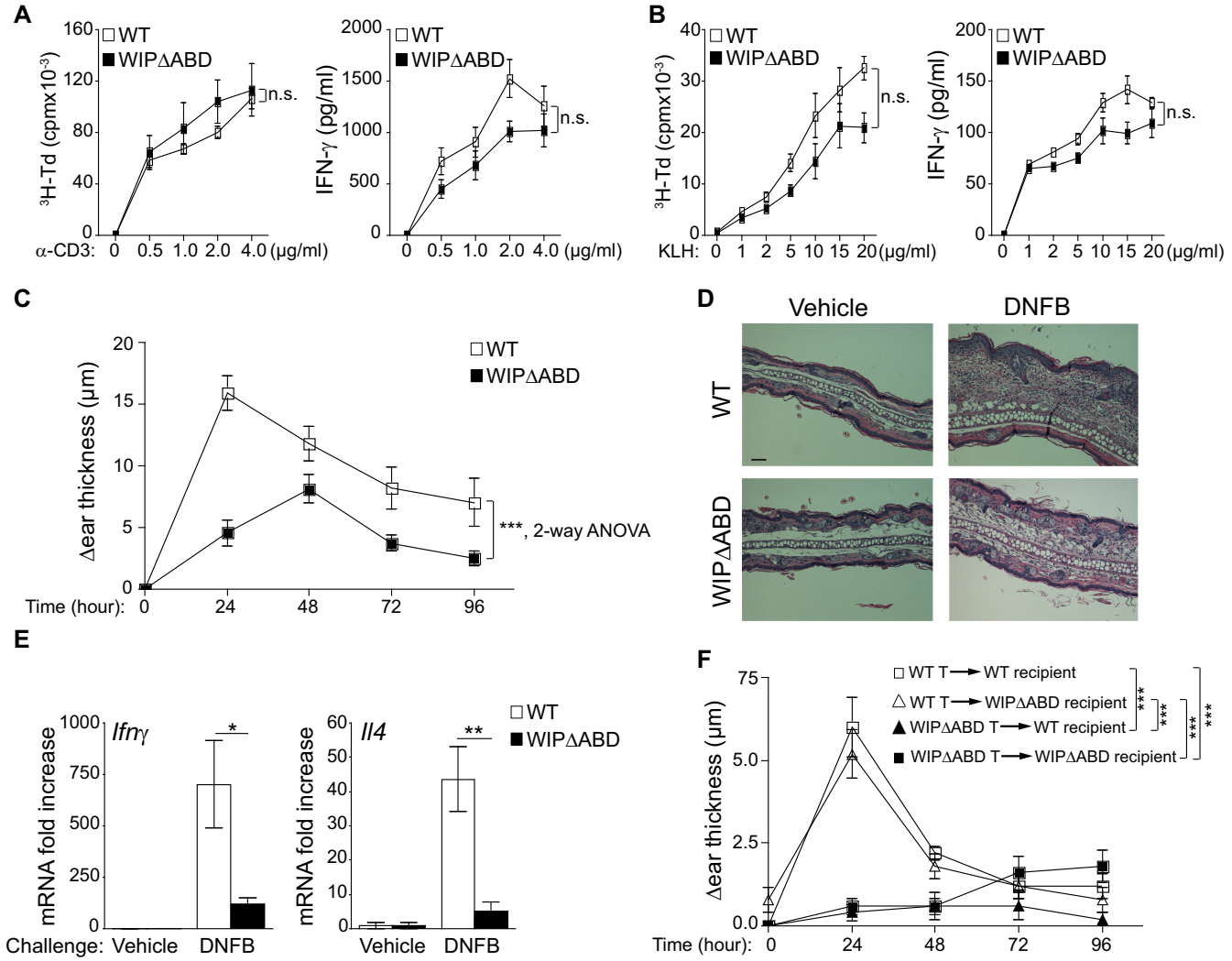

FIG 4 Defective CHS response in WIPΔABD mice. (A) Proliferation and IFN-γ production by T cells from WIPΔABD mice and WT controls stimulated with an increasing dose of plate-bound anti-CD3 MAb ($n = 6$ for each group). (B) Proliferation and IFN-γ production in response to KLH by splenocytes from WIPΔABD mice and WT controls i.p. immunized with KLH ($n = 6$ for each group). (C) CHS in WIPΔABD mice and WT controls measured as the difference in thickness between DNFB- and vehicle-challenged ears ($n = 12$ for each group). (D) Representative ear skin histology stained with H&E 24 h after challenge with DNFB or vehicle and then visualized by light microscopy. Bar, 50 μm. (E) *Ifnγ* and *Il4* mRNA expression in the ears of WIPΔABD mice and WT controls at 24 h after challenge with DNFB or vehicle. The data are represented as the fold increase in mRNA levels relative to vehicle-challenged ears of WT mice set at 1 ($n = 5$ for each group). (F) CHS in WIPΔABD and WT mice recipients of WT or WIPΔABD T cells purified from mice sensitized with DNFB ($n = 5$ for each group). Columns or squares and bars represent means ± the SEM. ***, $P < 0.0001$; **, $P < 0.01$; *, $P < 0.05$; n.s., not significant.

they adhered to a comparable extent to ICAM-1- and VCAM-1-coated surfaces under physiologic shear flow conditions (Fig. 6D). These results indicate that the ABD domain of WIP is not important for the ability of activated Ag-specific CD4$^+$ T cells to express molecules that mediate tethering and adhesion to endothelial cells and migration to the skin.

Seven days after adoptive transfer of activated CD4$^+$ DO11.10 T cells to WT recipients and i.d. injection of OVA or PBS into their ears, the ear cells were examined for the presence of CD4$^+$ KJ1-26$^+$ donor cells. As expected, CD4$^+$ KJ1-26$^+$ cells from WT donors accumulated significantly more in OVA-challenged than in PBS-challenged recipient ears (Fig. 6E and F). However, there was significantly less accumulation of CD4$^+$ KJ1-26$^+$ cells from WIPΔABD donors in OVA-challenged ears of WT recipients. Furthermore, the percentage of CD4$^+$ KJ1-26$^+$ ear cells that underwent cell division, as determined by the dilution of CellTrace Violet, and the percentage of CD4$^+$ KJ1-26$^+$ ear cells that were annexin V$^+$, an indicator of apoptosis, were comparable in recipients of WIPΔABD and WT transgenic T cells (Fig. 6G). This indicates that the decrease in WIPΔABD cells infiltrating the ears of WT recipients is not due to decreased proliferation or increased cell death at the site of Ag challenge. Taken together, these results demonstrate that the ABD of WIP plays an important role in the homing of CD4$^+$ T effector cells to cutaneous sites of Ag challenge.

We also tested the potential contribution of non-T cells to the defective ability of WIPΔABD mice to mount an inflammatory response to Ag challenge. OVA-stimulated WT CD4$^+$ DO11.10 cells were adoptively transferred to WIPΔABD and WT recipients, which were challenged with i.d. injection of OVA or PBS in the

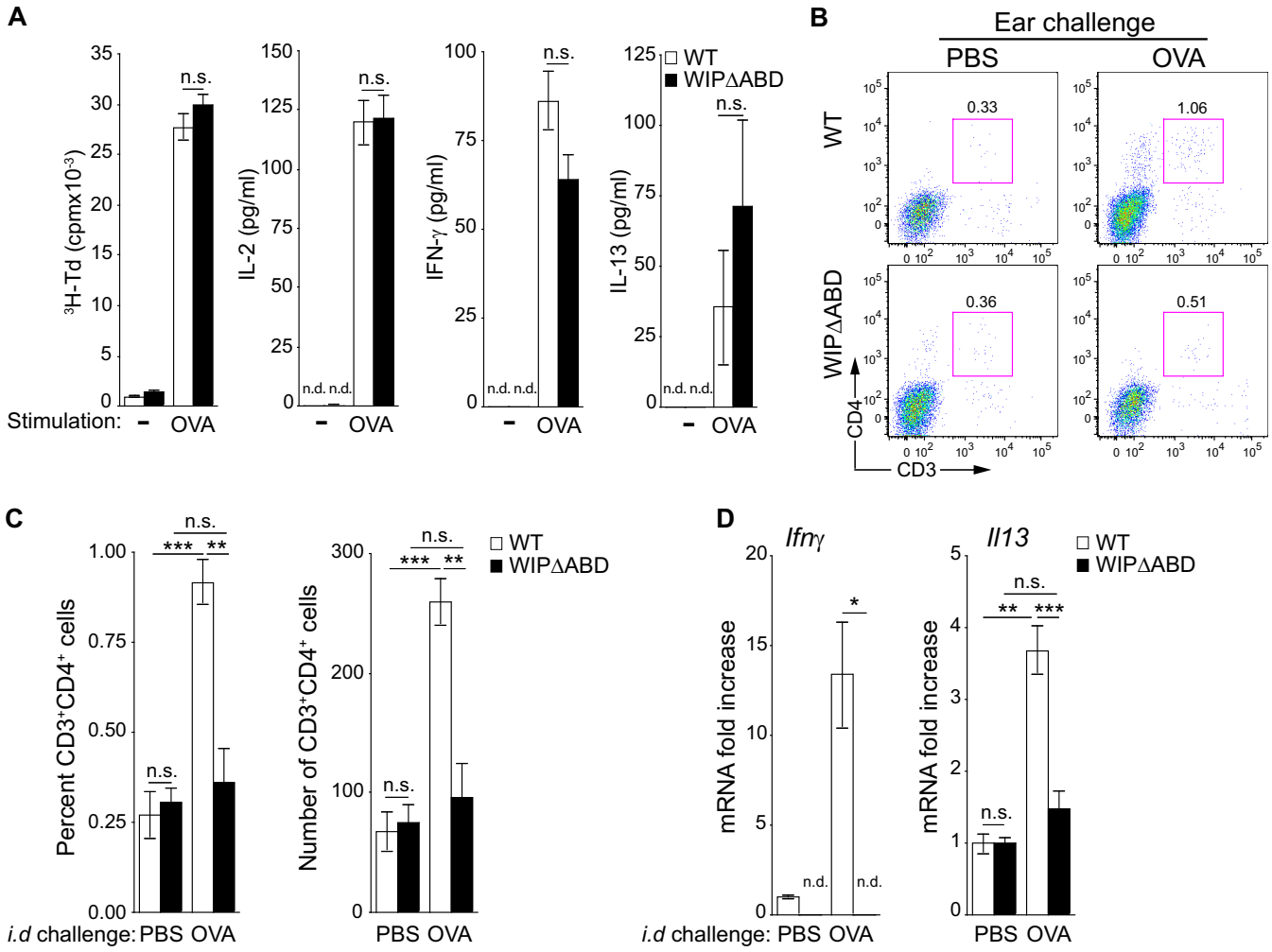

FIG 5 Defective accumulation of CD3$^+$ CD4$^+$ T cells in cutaneous sites of secondary Ag challenge in WIPΔABD mice. (A) Proliferation and secretion of IL-2, IFN-γ, and IL-13 in response to OVA by splenocytes from WIPΔABD mice and WT controls EC-immunized with OVA ($n = 5$ for each group). (B) Representative FACS analysis of CD3$^+$ CD4$^+$ cells in ears of WIPΔABD mice and WT controls 7 days following i.d. challenge with $OVA_{323-339}$ peptide or PBS as a control. (C) Percentages and numbers of CD3$^+$ CD4$^+$ cells in ears of WIPΔABD mice and WT controls 7 days after i.d. challenge with $OVA_{323-339}$ peptide or PBS as a control ($n = 5$ for each group). (D) *Ifn*γ and *Il13* mRNA expression in the ears of WIPΔABD mice and WT controls 7 days after i.d. challenge with $OVA_{323-339}$ peptide or PBS as a control. The data are represented as the fold increase in mRNA levels relative to PBS-challenged ears of WT mice set at 1 ($n = 5$ for each group). n.d., not detected. Columns and bars represent means ± the SEM. ***, $P < 0.001$; **, $P < 0.01$; *, $P < 0.05$; n.s., not significant.

ears. Seven days later, there was no significant difference in the accumulation of WT CD4$^+$ KJ1-26$^+$ cells in OVA-challenged ears of WIPΔABD and WT recipients (see Fig. S6 in the supplemental material). These findings suggest that non-T cells do not contribute significantly to the defective accumulation of T effector cells at sites of cutaneous challenge in WIPΔABD mice.

DISCUSSION

The results presented reveal that WIP binding to actin is essential for the integrity of the T cell actin cytoskeleton and for T cell migration into tissues.

The WIP mutant expressed by the WIPΔABD knock-in mice had the predicted molecular weight and interacted normally with WASp but demonstrated significantly decreased cosedimentation with F-actin in the high-speed centrifugation pellet of cell lysates. The residual presence of the mutant WIP in the pellet could be due to its binding to cytoskeletal proteins other than F-actin, such as myosin IIA (34), and/or to indirect interaction with F-actin. F-actin levels were significantly decreased in T cells from WIPΔABD mice. This was evidenced by the decrease in the amount of actin that sedimented in the high-speed centrifugation pellet of cell lysates and by the diminished intracellular F-actin content determined by flow cytometry. In contrast to the decreased intracellular F-actin content, the magnitude of the rise in cellular F-actin content after TCR/CD3 or CCR7 ligation was comparable in T cells from WIPΔABD mice and WT controls. These observations indicate that WIP binding to F-actin is important for the stability of F-actin in T cells and are concordant with our earlier *in vitro* finding that WIP stabilizes F-actin (19); however, the ABD is not critical for stimulation-induced F-actin polymerization in T cells.

WIPΔABD T cells spread poorly over anti-CD3-coated coverslips, displayed smaller pseudopodia, and were less motile than WT T cells. They also had a severely disrupted cortical actin cyto-

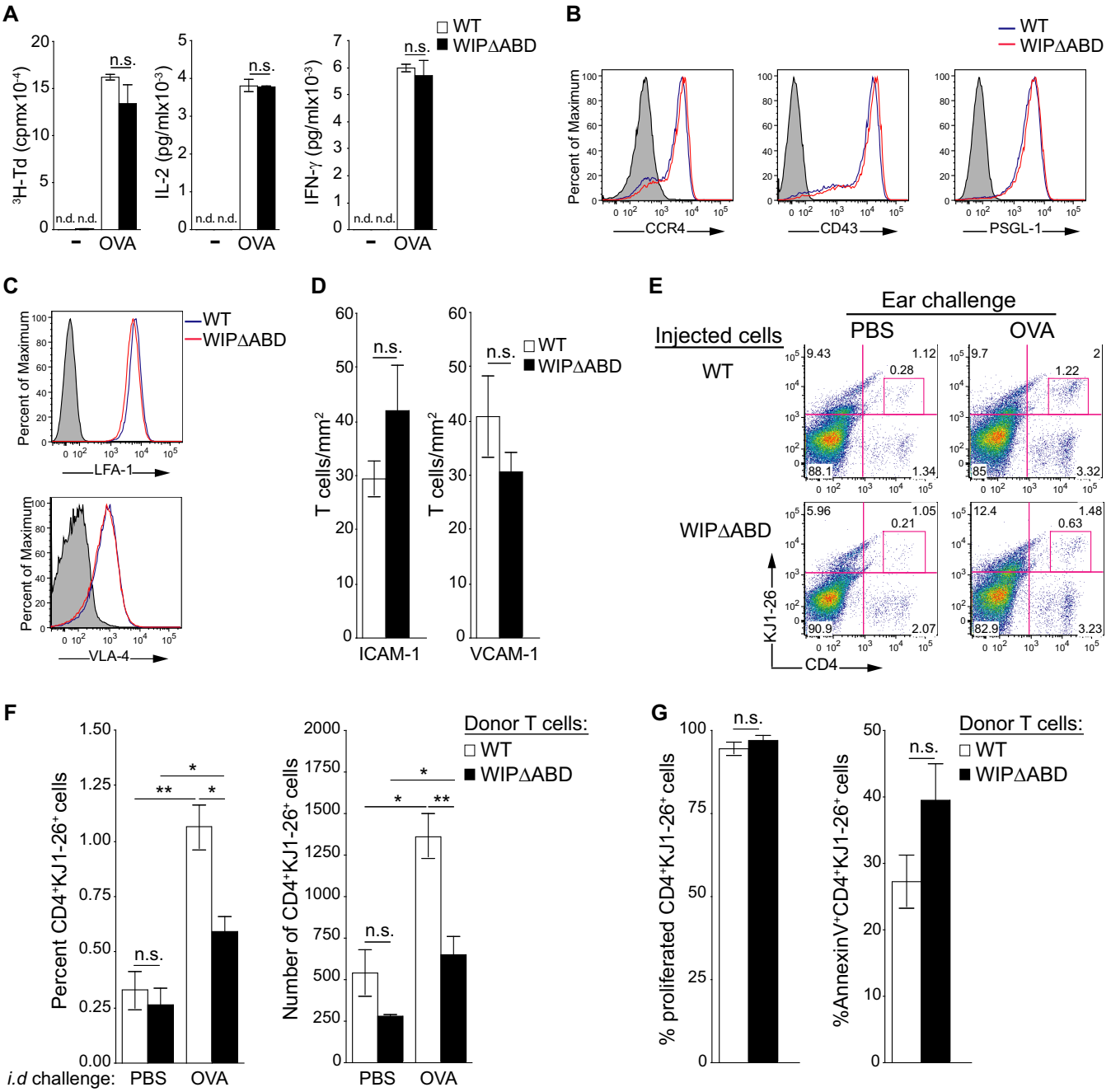

FIG 6 Defective homing of adoptively transferred WIPΔABD CD4$^+$ T cells to cutaneous sites of Ag challenge in WT recipient mice. (A) Tritiated thymidine (^{3}H-Td) proliferation and IL-2 and IFN-γ production by splenocytes from WIPΔABD and WT mice on the DO11.10 background after stimulation with OVA ($n = 5$ for each group). n.d., not detected. (B and C) Representative FACS analysis of OVA-stimulated splenic CD4$^+$ T cells from WIPΔABD and WT mice on the DO11.10 background for surface expression of CCR4, CD43, and PSGL-1 (B) and integrins LFA-1 and VLA-4 (C) ($n = 5$ for each group). The solid gray curve in the histogram represents the isotype control. (D) Adhesion of OVA-stimulated splenic CD4$^+$ T cells from WIPΔABD and WT mice on the DO11.10 background to ICAM-1 and VCAM-1 under conditions of physiologic shear stress flow (1 dyn/cm^2; $n = 2$ for each group). (E) Representative FACS analysis of CD4$^+$ KJ1-26$^+$ cells in OVA- and PBS-challenged ears from WT recipients of OVA-stimulated CD4$^+$ cells derived from DO11.10 WIPΔABD or WT mice. (F) Percentages and numbers of CD4$^+$ KJ1-26$^+$ cells in OVA- and PBS-challenged ears from WT recipients of OVA-stimulated CD4$^+$ cells derived from DO11.10 WIPΔABD or WT mice ($n = 5$ for each group). (G) Percentages of cells that have proliferated, as determined by dilution of CellTrace Violet (left panel), and of annexin V$^+$ cells (right panel) among CD4$^+$ KJ1-26$^+$ cells in OVA-challenged ears from WT recipients of OVA-stimulated CD4$^+$ cells derived from DO11.10 WIPΔABD or WT mice ($n = 4$ for each group). Columns and bars represent means ± the SEM. **, $P < 0.01$; *, $P < 0.05$; n.s., not significant.

skeleton. We previously showed that the cortical actin cytoskeleton is disrupted in T cells from *Wipf1*$^{-/-}$ mice but not in T cells from *Wasp*$^{-/-}$ mice (14, 16). Since *Wipf1*$^{-/-}$ mice express virtually no WASp, it had not been previously possible to determine whether the lack of WIP alone or the lack of both WIP and WASp caused the disruption in the cortical actin cytoskeleton in *Wipf1*$^{-/-}$ T cells. Given the similar disruption of the cortical actin cytoskeleton in WIPΔABD and *Wipf1*$^{-/-}$ mice, our results

strongly indicate that WIP, and not WASp, is essential for the integrity of the actin cytoskeleton and that the ABD plays a critical role in this function.

T cells from WIPΔABD mice displayed severely impaired chemotaxis to CCL19 and SDF-1α *in vitro*, and significantly decreased homing to LNs *in vivo*. Consistent with this homing defect, T cell numbers in the LNs of WIPΔABD mice were significantly decreased. Chemotaxis to SDF-1α is significantly impaired in T cells from *Wipf1*$^{-/-}$ mice but not in T cells from *Wasp*$^{-/-}$ mice (15). However, T cell homing to LN is impaired in both strains, and T cell transendothelial migration is impaired in *Wasp*$^{-/-}$ T cells (15, 35). Taken together, these results indicate that WIP, but not WASp, is essential for chemotaxis to SDF-1α *in vitro* by virtue of its ability to bind and stabilize F-actin. In contrast, both WASp, which is important for *de novo* actin polymerization in T cells (4, 36), and WIP binding to F-actin, which is essential for the integrity of the actin cytoskeleton, are important for the migration of T cells into LNs.

TCR-mediated activation of WIPΔABD T cells was intact. In contrast, T cells from *Wipf1*$^{-/-}$ mice, but not T cells from *Wasp*$^{-/-}$ mice, failed to proliferate in response to Ag stimulation and to respond to IL-2, although they secreted normal amounts of IL-2 (16). Given that T cells from WIPΔABD and *Wipf1*$^{-/-}$ mice have similar cytoskeletal abnormalities, our results suggest that WIP domains other than the ABD are important for TCR-mediated T cell activation.

In spite of a normal T cell response to i.p. and EC immunization with Ag, WIPΔABD mice had significantly impaired delayed CHS reaction to hapten. Adoptive-transfer experiments revealed that T cells were the major contributors to the impaired CHS in WIPΔABD mice. Given our previous observations that CHS is deficient in *Wipf1*$^{-/-}$ mice, but intact in *Wasp*$^{-/-}$ mice (16), our results indicate that the ABD of WIP is essential for the development of CHS.

WIPΔABD mice EC-sensitized with OVA had an impaired response to cutaneous Ag challenge at a secondary site, despite a normal systemic Ag-specific T cell response. We directly demonstrated that Ag-specific CD4$^+$ T effector cells from WIPΔABD mice are defective in their ability to home to sites of cutaneous Ag challenge. *In vitro*-activated OVA TCR transgenic CD4$^+$ T cells from WIPΔABD-DO11.10 mice were normal in their ability to proliferate, secrete cytokines, express selectin ligands, integrins, and CCR4, and adhered normally to ICAM-1- and VCAM-1-coated surfaces under physiologic shear flow conditions. However, they were deficient in their ability to accumulate in the skin of recipients that have been challenged by the i.d. injection of OVA. Their impaired accumulation in OVA-challenged skin was not the result of decreased proliferation or increased apoptosis. We also demonstrated that there was no significant difference between the accumulation of OVA TCR transgenic T cells from WT mice in the OVA-challenged ears of WIPΔABD and WT recipients, indicating that non-T cells do not play a significant role in the homing defect observed in WIPΔABD mice.

In summary, we have demonstrated that WIP binding to actin maintains the integrity of the actin cytoskeleton and promotes T cell migration, independently of its role in stabilizing WASp. Dissociating these two functions was previously not possible because of the susceptibility of WASp to degradation in the absence of WIP. Based on our findings, we propose a model in which WIP plays dual and complementary functions in T cells that are essential for maintaining actin cytoskeleton integrity and promoting migration: it stabilizes WASp, which drives *de novo* actin polymerization, and stabilizes newly synthesized actin filaments. Strategies aimed at disrupting WIP binding to actin to block T cell homing to inflamed tissues could be of therapeutic value in inflammatory diseases.

ACKNOWLEDGMENTS

We thank John Manis for useful advice and Talal Chatila and Hans Oetgen for critically reading the manuscript.

This study was supported by a grant from the Perkin foundation to M.J.M. and by National Institutes of Health grants 5PO1HL059561 to R.S.G., K99-HL097406 to P.A., and PO1 HL36028 to F.W.L.

We declare that no conflicts of interest exist.

REFERENCES

1. **Vicente-Manzanares M, Sancho D, Yanez-Mo M, Sanchez-Madrid F.** 2002. The leukocyte cytoskeleton in cell migration and immune interactions. Int. Rev. Cytol. **216:**233–289. http://dx.doi.org/10.1016/S0074-7696(02)16007-4.
2. **Dupre L, Aiuti A, Trifari S, Martino S, Saracco P, Bordignon C, Roncarolo MG.** 2002. Wiskott-Aldrich syndrome protein regulates lipid raft dynamics during immunological synapse formation. Immunity **17:**157–166. http://dx.doi.org/10.1016/S1074-7613(02)00360-6.
3. **Fooksman DR, Vardhana S, Vasiliver-Shamis G, Liese J, Blair DA, Waite J, Sacristan C, Victora GD, Zanin-Zhorov A, Dustin ML.** 2010. Functional anatomy of T cell activation and synapse formation. Annu. Rev. Immunol. **28:**79–105. http://dx.doi.org/10.1146/annurev-immunol-030409-101308.
4. **Gallego MD, Santamaria M, Pena J, Molina IJ.** 1997. Defective actin reorganization and polymerization of Wiskott-Aldrich T cells in response to CD3-mediated stimulation. Blood **90:**3089–3097.
5. **Haddad E, Zugaza JL, Louache F, Debili N, Crouin C, Schwarz K, Fischer A, Vainchenker W, Bertoglio J.** 2001. The interaction between Cdc42 and WASP is required for SDF-1-induced T-lymphocyte chemotaxis. Blood **97:**33–38. http://dx.doi.org/10.1182/blood.V97.1.33.
6. **Krzewski K, Chen X, Strominger JL.** 2008. WIP is essential for lytic granule polarization and NK cell cytotoxicity. Proc. Natl. Acad. Sci. U. S. A. **105:**2568–2573. http://dx.doi.org/10.1073/pnas.0711593105.
7. **Orange JS, Ramesh N, Remold-O'Donnell E, Sasahara Y, Koopman L, Byrne M, Bonilla FA, Rosen FS, Geha RS, Strominger JL.** 2002. Wiskott-Aldrich syndrome protein is required for NK cell cytotoxicity and colocalizes with actin to NK cell-activating immunologic synapses. Proc. Natl. Acad. Sci. U. S. A. **99:**11351–11356. http://dx.doi.org/10.1073/pnas.162376099.
8. **Rohatgi R, Ma L, Miki H, Lopez M, Kirchhausen T, Takenawa T, Kirschner MW.** 1999. The interaction between N-WASP and the Arp2/3 complex links Cdc42-dependent signals to actin assembly. Cell **97:**221–231. http://dx.doi.org/10.1016/S0092-8674(00)80732-1.
9. **de la Fuente MA, Sasahara Y, Calamito M, Anton IM, Elkhal A, Gallego MD, Suresh K, Siminovitch K, Ochs HD, Anderson KC, Rosen FS, Geha RS, Ramesh N.** 2007. WIP is a chaperone for Wiskott-Aldrich syndrome protein (WASP). Proc. Natl. Acad. Sci. U. S. A. **104:**926–931. http://dx.doi.org/10.1073/pnas.0610275104.
10. **Ramesh N, Anton IM, Hartwig JH, Geha RS.** 1997. WIP, a protein associated with Wiskott-Aldrich syndrome protein, induces actin polymerization and redistribution in lymphoid cells. Proc. Natl. Acad. Sci. U. S. A. **94:**14671–14676. http://dx.doi.org/10.1073/pnas.94.26.14671.
11. **Lanzi G, Moratto D, Vairo D, Masneri S, Delmonte O, Paganini T, Parolini S, Tabellini G, Mazza C, Savoldi G, Montin D, Martino S, Tovo P, Pessach IM, Massaad MJ, Ramesh N, Porta F, Plebani A, Notarangelo LD, Geha RS, Giliani S.** 2012. A novel primary human immunodeficiency due to deficiency in the WASP-interacting protein WIP. J. Exp. Med. **209:**29–34. http://dx.doi.org/10.1084/jem.20110896.
12. **Massaad MJ, Ramesh N, Geha RS.** 2013. Wiskott-Aldrich syndrome: a comprehensive review. Ann. N. Y. Acad. Sci. **1285:**26–43. http://dx.doi.org/10.1111/nyas.12049.
13. **Massaad MJ, Ramesh N, Le Bras S, Giliani S, Notarangelo LD, Al-Herz W, Geha RS.** 2011. A peptide derived from the Wiskott-Aldrich syndrome

(WAS) protein-interacting protein (WIP) restores WAS protein level and actin cytoskeleton reorganization in lymphocytes from patients with WAS mutations that disrupt WIP binding. J. Allergy Clin. Immunol. **127:**998–1005 e1001-1002. http://dx.doi.org/10.1016/j.jaci.2011.01.015.

14. **Anton IM, de la Fuente MA, Sims TN, Freeman S, Ramesh N, Hartwig JH, Dustin ML, Geha RS.** 2002. WIP deficiency reveals a differential role for WIP and the actin cytoskeleton in T and B cell activation. Immunity **16:**193–204. http://dx.doi.org/10.1016/S1074-7613(02)00268-6.
15. **Gallego MD, de la Fuente MA, Anton IM, Snapper S, Fuhlbrigge R, Geha RS.** 2006. WIP and WASP play complementary roles in T cell homing and chemotaxis to SDF-1α. Int. Immunol. **18:**221–232. http://dx.doi.org/10.1093/intimm/dxh310.
16. **Le Bras S, Massaad M, Koduru S, Kumar L, Oyoshi MK, Hartwig J, Geha RS.** 2009. WIP is critical for T cell responsiveness to IL-2. Proc. Natl. Acad. Sci. U. S. A. **106:**7519–7524. http://dx.doi.org/10.1073/pnas.0806410106.
17. **Anton IM, Saville SP, Byrne MJ, Curcio C, Ramesh N, Hartwig JH, Geha RS.** 2003. WIP participates in actin reorganization and ruffle formation induced by PDGF. J. Cell Sci. **116:**2443–2451. http://dx.doi.org/10.1242/jcs.00433.
18. **Van Troys M, Dewitte D, Goethals M, Carlier MF, Vandekerckhove J, Ampe C.** 1996. The actin binding site of thymosin beta 4 mapped by mutational analysis. EMBO J. **15:**201–210.
19. **Martinez-Quiles N, Rohatgi R, Anton IM, Medina M, Saville SP, Miki H, Yamaguchi H, Takenawa T, Hartwig JH, Geha RS, Ramesh N.** 2001. WIP regulates N-WASP-mediated actin polymerization and filopodium formation. Nat. Cell Biol. **3:**484–491. http://dx.doi.org/10.1038/35074551.
20. **Vetterkind S, Miki H, Takenawa T, Klawitz I, Scheidtmann KH, Preuss U.** 2002. The rat homologue of Wiskott-Aldrich syndrome protein (WASP)-interacting protein (WIP) associates with actin filaments, recruits N-WASP from the nucleus, and mediates mobilization of actin from stress fibers in favor of filopodia formation. J. Biol. Chem. **277:**87–95. http://dx.doi.org/10.1074/jbc.M104555200.
21. **Koduru S, Massaad M, Wilbur C, Kumar L, Geha R, Ramesh N.** 2007. A novel anti-WIP monoclonal antibody detects an isoform of WIP that lacks the WASP binding domain. Biochem. Biophys. Res. Commun. **353:**875–881. http://dx.doi.org/10.1016/j.bbrc.2006.12.079.
22. **Alcaide P, Maganto-Garcia E, Newton G, Travers R, Croce KJ, Bu DX, Luscinskas FW, Lichtman AH.** 2012. Difference in Th1 and Th17 lymphocyte adhesion to endothelium. J. Immunol. **188:**1421–1430. http://dx.doi.org/10.4049/jimmunol.1101647.
23. **Parsey MV, Lewis GK.** 1993. Actin polymerization and pseudopod reorganization accompany anti-CD3-induced growth arrest in Jurkat T cells. J. Immunol. **151:**1881–1893.
24. **Bunnell SC, Kapoor V, Trible RP, Zhang W, Samelson LE.** 2001. Dynamic actin polymerization drives T cell receptor-induced spreading: a role for the signal transduction adaptor LAT. Immunity **14:**315–329. http://dx.doi.org/10.1016/S1074-7613(01)00112-1.
25. **Blades MC, Manzo A, Ingegnoli F, Taylor PR, Panayi GS, Irjala H, Jalkanen S, Haskard DO, Perretti M, Pitzalis C.** 2002. Stromal cell-derived factor 1 (CXCL12) induces human cell migration into human lymph nodes transplanted into SCID mice. J. Immunol. **168:**4308–4317. http://dx.doi.org/10.4049/jimmunol.168.9.4308.
26. **Phillips R, Ager A.** 2002. Activation of pertussis toxin-sensitive CXCL12 (SDF-1) receptors mediates transendothelial migration of T lymphocytes across lymph node high endothelial cells. Eur. J. Immunol. **32:**837–847. http://dx.doi.org/10.1002/1521-4141(200203)32:3<837::AID-IMMU837>3.0.CO;2-Q.
27. **Gunn MD, Kyuwa S, Tam C, Kakiuchi T, Matsuzawa A, Williams LT, Nakano H.** 1999. Mice lacking expression of secondary lymphoid organ chemokine have defects in lymphocyte homing and dendritic cell localization. J. Exp. Med. **189:**451–460. http://dx.doi.org/10.1084/jem.189.3.451.
28. **Gunn MD, Tangemann K, Tam C, Cyster JG, Rosen SD, Williams LT.** 1998. A chemokine expressed in lymphoid high endothelial venules promotes the adhesion and chemotaxis of naive T lymphocytes. Proc. Natl. Acad. Sci. U. S. A. **95:**258–263. http://dx.doi.org/10.1073/pnas.95.1.258.
29. **Gorbachev AV, Fairchild RL.** 2004. $CD4^+$ T cells regulate $CD8^+$ T cell-mediated cutaneous immune responses by restricting effector T cell development through a Fas ligand-dependent mechanism. J. Immunol. **172:**2286–2295. http://dx.doi.org/10.4049/jimmunol.172.4.2286.
30. **Wang B, Fujisawa H, Zhuang L, Freed I, Howell BG, Shahid S, Shivji GM, Mak TW, Sauder DN.** 2000. $CD4^+$ Th1 and $CD8^+$ type 1 cytotoxic T cells both play a crucial role in the full development of contact hypersensitivity. J. Immunol. **165:**6783–6790. http://dx.doi.org/10.4049/jimmunol.165.12.6783.
31. **Spergel JM, Mizoguchi E, Brewer JP, Martin TR, Bhan AK, Geha RS.** 1998. Epicutaneous sensitization with protein antigen induces localized allergic dermatitis and hyperresponsiveness to methacholine after single exposure to aerosolized antigen in mice. J. Clin. Invest. **101:**1614–1622. http://dx.doi.org/10.1172/JCI1647.
32. **Henri S, Guilliams M, Poulin LF, Tamoutounour S, Ardouin L, Dalod M, Malissen B.** 2010. Disentangling the complexity of the skin dendritic cell network. Immunol. Cell Biol. **88:**366–375. http://dx.doi.org/10.1038/icb.2010.34.
33. **Roediger B, Ng LG, Smith AL, Fazekas de St Groth B, Weninger W.** 2008. Visualizing dendritic cell migration within the skin. Histochem. Cell Biol. **130:**1131–1146. http://dx.doi.org/10.1007/s00418-008-0531-7.
34. **Krzewski K, Chen X, Orange JS, Strominger JL.** 2006. Formation of a WIP-, WASp-, actin-, and myosin IIA-containing multiprotein complex in activated NK cells and its alteration by KIR inhibitory signaling. J. Cell Biol. **173:**121–132. http://dx.doi.org/10.1083/jcb.200509076.
35. **Carman CV, Sage PT, Sciuto TE, de la Fuente MA, Geha RS, Ochs HD, Dvorak HF, Dvorak AM, Springer TA.** 2007. Transcellular diapedesis is initiated by invasive podosomes. Immunity **26:**784–797. http://dx.doi.org/10.1016/j.immuni.2007.04.015.
36. **Snapper SB, Rosen FS, Mizoguchi E, Cohen P, Khan W, Liu CH, Hagemann TL, Kwan SP, Ferrini R, Davidson L, Bhan AK, Alt FW.** 1998. Wiskott-Aldrich syndrome protein-deficient mice reveal a role for WASP in T but not B cell activation. Immunity **9:**81–91. http://dx.doi.org/10.1016/S1074-7613(00)80590-7.